EUROPEAN ORGANIZATION FOR NUCLEAR RESEARCH

CERN–PPE/96-77

12 June 1996

Measurement of Inclusive $K^{*0}(892)$, $\phi(1020)$ and $K_2^{*0}(1430)$ Production in Hadronic Z Decays

DELPHI Collaboration

Abstract

The inclusive production of the neutral vector mesons $K^{*0}(892)$ and $\phi(1020)$, and of the tensor meson $K_2^{*0}(1430)$, in hadronic decays of the Z has been measured by the DELPHI detector at LEP. The average production rates per hadronic Z decay have been determined to be 0.77 ± 0.08 $K^{*0}(892)$, 0.104 ± 0.008 $\phi(1020)$ and 0.079 ± 0.040 $K_2^{*0}(1430)$. The ratio of the tensor-to-vector meson production yields, $\langle K_2^{*0}(1430)\rangle/\langle K^{*0}(892)\rangle = 0.10 \pm 0.05$, is smaller than the $\langle f_2(1270)\rangle/\langle \rho^0(770)\rangle$ and $\langle f_2'(1525)\rangle/\langle \phi(1020)\rangle$ ratios measured by DELPHI. The production rates and differential cross sections are compared with the predictions of JETSET 7.4 tuned to the DELPHI data and of HERWIG 5.8. The $K^{*0}(892)$ and $\phi(1020)$ data are compatible with model predictions, but a large disagreement is observed for the $K_2^{*0}(1430)$.

(To be submitted to Zeit. für Physik C)

P.Abreu[21], W.Adam[50], T.Adye[37], E.Agasi[31], I.Ajinenko[42], R.Aleksan[39], G.D.Alekseev[16], R.Alemany[49], P.P.Allport[22], S.Almehed[24], U.Amaldi[9], S.Amato[47], A.Andreazza[28], M.L.Andrieux[14], P.Antilogus[9], W-D.Apel[17], Y.Arnoud[39], B.Åsman[44], J-E.Augustin[25], A.Augustinus[9], P.Baillon[9], P.Bambade[19], R.Barate[14], M.Barbi[47], D.Y.Bardin[16], A.Baroncelli[40], O.Barring[24], J.A.Barrio[26], W.Bartl[50], M.J.Bates[37], M.Battaglia[15], M.Baubillier[23], J.Baudot[39], K-H.Becks[52], M.Begalli[6], P.Beilliere[8], Yu.Belokopytov[9,53], K.Belous[42], A.C.Benvenuti[5], M.Berggren[47], D.Bertini[25], D.Bertrand[2], F.Bianchi[45], M.Bigi[45], M.S.Bilenky[16], P.Billoir[23], D.Bloch[10], M.Blume[52], T.Bolognese[39], M.Bonesini[28], W.Bonivento[28], P.S.L.Booth[22], C.Bosio[40], O.Botner[48], E.Boudinov[31], B.Bouquet[19], C.Bourdarios[9], T.J.V.Bowcock[22], M.Bozzo[13], P.Branchini[40], K.D.Brand[36], T.Brenke[52], R.A.Brenner[15], C.Bricman[2], R.C.A.Brown[9], P.Bruckman[18], J-M.Brunet[8], L.Bugge[33], T.Buran[33], T.Burgsmueller[52], P.Buschmann[52], A.Buys[9], S.Cabrera[49], M.Caccia[28], M.Calvi[28], A.J.Camacho Rozas[41], T.Camporesi[9], V.Canale[38], M.Canepa[13], K.Cankocak[44], F.Cao[2], F.Carena[9], L.Carroll[22], C.Caso[13], M.V.Castillo Gimenez[49], A.Cattai[9], F.R.Cavallo[5], V.Chabaud[9], M.Chapkin[42], Ph.Charpentier[9], L.Chaussard[25], P.Checchia[36], G.A.Chelkov[16], M.Chen[2], R.Chierici[45], P.Chliapnikov[42], P.Chochula[7], V.Chorowicz[9], V.Cindro[43], P.Collins[9], J.L.Contreras[19], R.Contri[13], E.Cortina[49], G.Cosme[19], F.Cossutti[46], H.B.Crawley[1], D.Crennell[37], G.Crosetti[13], J.Cuevas Maestro[34], S.Czellar[15], E.Dahl-Jensen[29], J.Dahm[52], B.Dalmagne[19], M.Dam[29], G.Damgaard[29], P.D.Dauncey[37], M.Davenport[9], W.Da Silva[23], C.Defoix[8], A.Deghorain[2], G.Della Ricca[46], P.Delpierre[27], N.Demaria[35], A.De Angelis[9], W.De Boer[17], S.De Brabandere[2], C.De Clercq[2], C.De La Vaissiere[23], B.De Lotto[46], A.De Min[36], L.De Paula[47], C.De Saint-Jean[39], H.Dijkstra[9], L.Di Ciaccio[38], F.Djama[10], J.Dolbeau[8], M.Donszelmann[9], K.Doroba[51], M.Dracos[10], J.Drees[52], K.-A.Drees[52], M.Dris[32], J-D.Durand[25], D.Edsall[1], R.Ehret[17], G.Eigen[4], T.Ekelof[48], G.Ekspong[44], M.Elsing[52], J-P.Engel[10], B.Erzen[43], M.Espirito Santo[21], E.Falk[24], D.Fassouliotis[32], M.Feindt[9], A.Ferrer[49], S.Fichet[23], T.A.Filippas[32], A.Firestone[1], P.-A.Fischer[10], H.Foeth[9], E.Fokitis[32], F.Fontanelli[13], F.Formenti[9], B.Franek[37], P.Frenkiel[8], D.C.Fries[17], A.G.Frodesen[4], R.Fruhwirth[50], F.Fulda-Quenzer[19], J.Fuster[49], A.Galloni[22], D.Gamba[45], M.Gandelman[6], C.Garcia[49], J.Garcia[41], C.Gaspar[9], U.Gasparini[36], Ph.Gavillet[9], E.N.Gazis[32], D.Gele[10], J-P.Gerber[10], L.Gerdyukov[42], M.Gibbs[22], R.Gokieli[51], B.Golob[43], G.Gopal[37], L.Gorn[1], M.Gorski[51], Yu.Gouz[45,53], V.Gracco[13], E.Graziani[40], G.Grosdidier[19], K.Grzelak[51], S.Gumenyuk[28,53], P.Gunnarsson[44], M.Gunther[48], J.Guy[37], F.Hahn[9], S.Hahn[52], Z.Hajduk[18], A.Hallgren[48], K.Hamacher[52], W.Hao[31], F.J.Harris[35], V.Hedberg[24], R.Henriques[21], J.J.Hernandez[49], P.Herquet[2], H.Herr[9], T.L.Hessing[35], E.Higon[49], H.J.Hilke[9], T.S.Hill[1], S-O.Holmgren[44], P.J.Holt[35], D.Holthuizen[31], S.Hoorelbeke[2], M.Houlden[22], J.Hrubec[50], K.Huet[2], K.Hultqvist[44], J.N.Jackson[22], R.Jacobsson[44], P.Jalocha[18], R.Janik[7], Ch.Jarlskog[24], G.Jarlskog[24], P.Jarry[39], B.Jean-Marie[19], E.K.Johansson[44], L.Jonsson[24], P.Jonsson[24], C.Joram[9], P.Juillot[10], M.Kaiser[17], F.Kapusta[23], K.Karafasoulis[11], M.Karlsson[44], E.Karvelas[11], S.Katsanevas[3], E.C.Katsoufis[32], R.Keranen[4], Yu.Khokhlov[42], B.A.Khomenko[16], N.N.Khovanski[16], B.King[22], N.J.Kjaer[29], H.Klein[9], A.Klovning[4], P.Kluit[31], B.Koene[31], P.Kokkinias[11], M.Koratzinos[9], K.Korcyl[18], V.Kostioukhine[42], C.Kourkoumelis[3], O.Kouznetsov[13,16], P.-H.Kramer[52], M.Krammer[50], C.Kreuter[17], I.Kronkvist[24], Z.Krumstein[16], W.Krupinski[18], P.Kubinec[7], W.Kucewicz[18], K.Kurvinen[15], C.Lacasta[49], I.Laktineh[25], J.W.Lamsa[1], L.Lanceri[46], D.W.Lane[1], P.Langefeld[52], V.Lapin[42], I.Last[22], J-P.Laugier[39], R.Lauhakangas[15], G.Leder[50], F.Ledroit[14], V.Lefebure[2], C.K.Legan[1], R.Leitner[30], Y.Lemoigne[39], J.Lemonne[2], G.Lenzen[52], V.Lepeltier[19], T.Lesiak[18], J.Libby[35], D.Liko[50], R.Lindner[52], A.Lipniacka[36], I.Lippi[36], B.Loerstad[24], J.G.Loken[35], J.M.Lopez[41], D.Loukas[11], P.Lutz[39], L.Lyons[35], G.Maehlum[17], A.Maio[21], T.G.M.Malmgren[44], V.Malychev[16], F.Mandl[50], J.Marco[41], R.Marco[41], B.Marechal[47], M.Margoni[36], J-C.Marin[9], C.Mariotti[40], A.Markou[11], T.Maron[52], C.Martinez-Rivero[41], F.Martinez-Vidal[49], S.Marti i Garcia[49], F.Matorras[41], C.Matteuzzi[9], G.Matthiae[38], M.Mazzucato[36], M.Mc Cubbin[9], R.Mc Kay[1], R.Mc Nulty[22], J.Medbo[48], M.Merk[31], C.Meroni[28], S.Meyer[17], W.T.Meyer[1], M.Michelotto[36], E.Migliore[45], L.Mirabito[25], W.A.Mitaroff[50], U.Mjoernmark[24], T.Moa[44], R.Moeller[29], K.Moenig[9], M.R.Monge[13], P.Morettini[13], H.Mueller[17], L.M.Mundim[6], W.J.Murray[37], B.Muryn[18], G.Myatt[35], F.Naraghi[14], F.L.Navarria[5], S.Navas[49], K.Nawrocki[51], P.Negri[28], S.Nemecek[12], W.Neumann[52], N.Neumeister[50], R.Nicolaidou[3], B.S.Nielsen[29], M.Nieuwenhuizen[31], V.Nikolaenko[10], P.Niss[44], A.Nomerotski[36], A.Normand[35], M.Novak[12], W.Oberschulte-Beckmann[17], V.Obraztsov[42], A.G.Olshevski[16], A.Onofre[21], R.Orava[15], K.Osterberg[15], A.Ouraou[39], P.Paganini[19], M.Paganoni[9], P.Pages[10], R.Pain[23], H.Palka[18], Th.D.Papadopoulou[32], K.Papageorgiou[11], L.Pape[9], C.Parkes[35], F.Parodi[13], A.Passeri[40], M.Pegoraro[36], L.Peralta[21], H.Pernegger[50], M.Pernicka[50], A.Perrotta[5], C.Petridou[46], A.Petrolini[13], M.Petrovyck[28,53], H.T.Phillips[37], G.Piana[13], F.Pierre[39], M.Pimenta[21], S.Plaszczynski[19], O.Podobrin[17], M.E.Pol[6], G.Polok[18], P.Poropat[46], V.Pozdniakov[16], M.Prest[46], P.Privitera[38], N.Pukhaeva[16], A.Pullia[28], D.Radojicic[35], S.Ragazzi[28], H.Rahmani[32], J.Rames[12], P.N.Ratoff[20], A.L.Read[33], M.Reale[52], P.Rebecchi[19], N.G.Redaelli[28], M.Regler[50], D.Reid[9], P.B.Renton[35], L.K.Resvanis[3], F.Richard[19], J.Richardson[22], J.Ridky[12], G.Rinaudo[45], I.Ripp[39], A.Romero[45], I.Roncagliolo[13], P.Ronchese[36], L.Roos[14], E.I.Rosenberg[1], E.Rosso[9], P.Roudeau[19], T.Rovelli[5], W.Ruckstuhl[31], V.Ruhlmann-Kleider[39], A.Ruiz[41], K.Rybicki[18], H.Saarikko[15], Y.Sacquin[39], A.Sadovsky[16], O.Sahr[14], G.Sajot[14], J.Salt[49], J.Sanchez[26], M.Sannino[13], M.Schimmelpfennig[17], H.Schneider[17], U.Schwickerath[17], M.A.E.Schyns[52], G.Sciolla[45], F.Scuri[46], P.Seager[20], Y.Sedykh[16], A.M.Segar[35], A.Seitz[17], R.Sekulin[37], L.Serbelloni[38], R.C.Shellard[6], I.Siccama[31], P.Siegrist[39], S.Simonetti[39], F.Simonetto[36], A.N.Sisakian[16], B.Sitar[7], T.B.Skaali[33], G.Smadja[25], N.Smirnov[42], O.Smirnova[24], G.R.Smith[37], R.Sosnowski[51], D.Souza-Santos[6], T.Spassov[21], E.Spiriti[40], P.Sponholz[52], S.Squarcia[13], C.Stanescu[40], S.Stapnes[33], I.Stavitski[36], K.Stevenson[35], F.Stichelbaut[9], A.Stocchi[19], J.Strauss[50], R.Strub[10], B.Stugu[4], M.Szczekowski[51], M.Szeptycka[51], T.Tabarelli[28], J.P.Tavernet[23],

O.Tchikilev[42], J.Thomas[35], A.Tilquin[27], J.Timmermans[31], L.G.Tkatchev[16], T.Todorov[10], S.Todorova[10], D.Z.Toet[31], A.Tomaradze[2], B.Tome[21], A.Tonazzo[28], L.Tortora[40], G.Transtromer[24], D.Treille[9], W.Trischuk[9], G.Tristram[8], A.Trombini[19], C.Troncon[28], A.Tsirou[9], M-L.Turluer[39], I.A.Tyapkin[16], M.Tyndel[37], S.Tzamarias[22], B.Ueberschaer[52], O.Ullaland[9], V.Uvarov[42], G.Valenti[5], E.Vallazza[9], G.W.Van Apeldoorn[31], P.Van Dam[31], J.Van Eldik[31], N.Vassilopoulos[35], G.Vegni[28], L.Ventura[36], W.Venus[37], F.Verbeure[2], M.Verlato[36], L.S.Vertogradov[16], D.Vilanova[39], P.Vincent[25], L.Vitale[46], E.Vlasov[42], A.S.Vodopyanov[16], V.Vrba[12], H.Wahlen[52], C.Walck[44], F.Waldner[46], M.Weierstall[52], P.Weilhammer[9], C.Weiser[17], A.M.Wetherell[9], D.Wicke[52], J.H.Wickens[2], M.Wielers[17], G.R.Wilkinson[35], W.S.C.Williams[35], M.Winter[10], M.Witek[18], K.Woschnagg[48], K.Yip[35], O.Yushchenko[42], F.Zach[25], A.Zaitsev[42], A.Zalewska[9], P.Zalewski[51], D.Zavrtanik[43], E.Zevgolatakos[11], N.I.Zimin[16], M.Zito[39], D.Zontar[43], G.C.Zucchelli[44], G.Zumerle[36]

[1] Ames Laboratory and Department of Physics, Iowa State University, Ames IA 50011, USA
[2] Physics Department, Univ. Instelling Antwerpen, Universiteitsplein 1, B-2610 Wilrijk, Belgium
and IIHE, ULB-VUB, Pleinlaan 2, B-1050 Brussels, Belgium
and Faculté des Sciences, Univ. de l'Etat Mons, Av. Maistriau 19, B-7000 Mons, Belgium
[3] Physics Laboratory, University of Athens, Solonos Str. 104, GR-10680 Athens, Greece
[4] Department of Physics, University of Bergen, Allégaten 55, N-5007 Bergen, Norway
[5] Dipartimento di Fisica, Università di Bologna and INFN, Via Irnerio 46, I-40126 Bologna, Italy
[6] Centro Brasileiro de Pesquisas Físicas, rua Xavier Sigaud 150, RJ-22290 Rio de Janeiro, Brazil
and Depto. de Física, Pont. Univ. Católica, C.P. 38071 RJ-22453 Rio de Janeiro, Brazil
and Inst. de Física, Univ. Estadual do Rio de Janeiro, rua São Francisco Xavier 524, Rio de Janeiro, Brazil
[7] Comenius University, Faculty of Mathematics and Physics, Mlynska Dolina, SK-84215 Bratislava, Slovakia
[8] Collège de France, Lab. de Physique Corpusculaire, IN2P3-CNRS, F-75231 Paris Cedex 05, France
[9] CERN, CH-1211 Geneva 23, Switzerland
[10] Centre de Recherche Nucléaire, IN2P3 - CNRS/ULP - BP20, F-67037 Strasbourg Cedex, France
[11] Institute of Nuclear Physics, N.C.S.R. Demokritos, P.O. Box 60228, GR-15310 Athens, Greece
[12] FZU, Inst. of Physics of the C.A.S. High Energy Physics Division, Na Slovance 2, 180 40, Praha 8, Czech Republic
[13] Dipartimento di Fisica, Università di Genova and INFN, Via Dodecaneso 33, I-16146 Genova, Italy
[14] Institut des Sciences Nucléaires, IN2P3-CNRS, Université de Grenoble 1, F-38026 Grenoble Cedex, France
[15] Research Institute for High Energy Physics, SEFT, P.O. Box 9, FIN-00014 Helsinki, Finland
[16] Joint Institute for Nuclear Research, Dubna, Head Post Office, P.O. Box 79, 101 000 Moscow, Russian Federation
[17] Institut für Experimentelle Kernphysik, Universität Karlsruhe, Postfach 6980, D-76128 Karlsruhe, Germany
[18] Institute of Nuclear Physics and University of Mining and Metalurgy, Ul. Kawiory 26a, PL-30055 Krakow, Poland
[19] Université de Paris-Sud, Lab. de l'Accélérateur Linéaire, IN2P3-CNRS, Bât. 200, F-91405 Orsay Cedex, France
[20] School of Physics and Chemistry, University of Lancaster, Lancaster LA1 4YB, UK
[21] LIP, IST, FCUL - Av. Elias Garcia, 14-1°, P-1000 Lisboa Codex, Portugal
[22] Department of Physics, University of Liverpool, P.O. Box 147, Liverpool L69 3BX, UK
[23] LPNHE, IN2P3-CNRS, Universités Paris VI et VII, Tour 33 (RdC), 4 place Jussieu, F-75252 Paris Cedex 05, France
[24] Department of Physics, University of Lund, Sölvegatan 14, S-22363 Lund, Sweden
[25] Université Claude Bernard de Lyon, IPNL, IN2P3-CNRS, F-69622 Villeurbanne Cedex, France
[26] Universidad Complutense, Avda. Complutense s/n, E-28040 Madrid, Spain
[27] Univ. d'Aix - Marseille II - CPP, IN2P3-CNRS, F-13288 Marseille Cedex 09, France
[28] Dipartimento di Fisica, Università di Milano and INFN, Via Celoria 16, I-20133 Milan, Italy
[29] Niels Bohr Institute, Blegdamsvej 17, DK-2100 Copenhagen 0, Denmark
[30] NC, Nuclear Centre of MFF, Charles University, Areal MFF, V Holesovickach 2, 180 00, Praha 8, Czech Republic
[31] NIKHEF-H, Postbus 41882, NL-1009 DB Amsterdam, The Netherlands
[32] National Technical University, Physics Department, Zografou Campus, GR-15773 Athens, Greece
[33] Physics Department, University of Oslo, Blindern, N-1000 Oslo 3, Norway
[34] Dpto. Fisica, Univ. Oviedo, C/P. Pérez Casas, S/N-33006 Oviedo, Spain
[35] Department of Physics, University of Oxford, Keble Road, Oxford OX1 3RH, UK
[36] Dipartimento di Fisica, Università di Padova and INFN, Via Marzolo 8, I-35131 Padua, Italy
[37] Rutherford Appleton Laboratory, Chilton, Didcot OX11 OQX, UK
[38] Dipartimento di Fisica, Università di Roma II and INFN, Tor Vergata, I-00173 Rome, Italy
[39] CEA, DAPNIA/Service de Physique des Particules, CE-Saclay, F-91191 Gif-sur-Yvette Cedex, France
[40] Istituto Superiore di Sanità, Ist. Naz. di Fisica Nucl. (INFN), Viale Regina Elena 299, I-00161 Rome, Italy
[41] Instituto de Fisica de Cantabria (CSIC-UC), Avda. los Castros, S/N-39006 Santander, Spain, (CICYT-AEN93-0832)
[42] Inst. for High Energy Physics, Serpukov P.O. Box 35, Protvino, (Moscow Region), Russian Federation
[43] J. Stefan Institute and Department of Physics, University of Ljubljana, Jamova 39, SI-61000 Ljubljana, Slovenia
[44] Fysikum, Stockholm University, Box 6730, S-113 85 Stockholm, Sweden
[45] Dipartimento di Fisica Sperimentale, Università di Torino and INFN, Via P. Giuria 1, I-10125 Turin, Italy
[46] Dipartimento di Fisica, Università di Trieste and INFN, Via A. Valerio 2, I-34127 Trieste, Italy
and Istituto di Fisica, Università di Udine, I-33100 Udine, Italy
[47] Univ. Federal do Rio de Janeiro, C.P. 68528 Cidade Univ., Ilha do Fundão BR-21945-970 Rio de Janeiro, Brazil
[48] Department of Radiation Sciences, University of Uppsala, P.O. Box 535, S-751 21 Uppsala, Sweden
[49] IFIC, Valencia-CSIC, and D.F.A.M.N., U. de Valencia, Avda. Dr. Moliner 50, E-46100 Burjassot (Valencia), Spain
[50] Institut für Hochenergiephysik, Österr. Akad. d. Wissensch., Nikolsdorfergasse 18, A-1050 Vienna, Austria
[51] Inst. Nuclear Studies and University of Warsaw, Ul. Hoza 69, PL-00681 Warsaw, Poland
[52] Fachbereich Physik, University of Wuppertal, Postfach 100 127, D-42097 Wuppertal, Germany
[53] On leave of absence from IHEP Serpukhov

1 Introduction

With the large statistics presently accumulated by the LEP experiments, at least one state per isospin multiplet has been measured for the SU(3) pseudoscalar and vector meson nonets, and for the baryon octet and decuplet (for reviews, see [1,2]). This allowed tuning of a number of adjustable parameters in the QCD-based Monte Carlo models such as JETSET [3] or HERWIG [4] to get a reasonable description of the experimental data [5], thus obtaining useful information about the nature of the fragmentation process. Still, the numerous model parameters are often strongly correlated and their physical interpretation is not always obvious.

On the other hand, the precise LEP measurements have established new experimental regularities and provided new insights on hadron production mechanisms in e^+e^- annihilations. For the pseudoscalar and vector mesons, and for the baryon octet and decuplet, a universal and energy–independent mass dependence of the relative particle production rates has been observed [6]. Surprisingly similar behaviour was also established in pp collisions for particles not resulting from fragmentation of the incident proton [2,7]. Good agreement has also been observed between the LEP data, a recently proposed thermodynamical model [8], and the model of ref. [9].

It is therefore of interest to determine the production properties at LEP of other meson and baryon states composed of light (u, d, s) quarks, and especially of those with non-zero angular momentum between the quarks in view of their possibly different production dynamics. Here the experimental information is more limited and less precise. So far, only the measurements of the scalar, $f_0(975)$, and tensor, $f_2(1270)$, $\mathrm{K}_2^{*\pm}(1430)$ and $f_2'(1525)$, mesons have been reported by DELPHI [10,11], and of the tensor, $\mathrm{K}_2^{*0}(1430)$, meson by OPAL [12].

This paper presents new DELPHI results on $\phi(1020)$ and $\mathrm{K}_2^{*0}(1430)$ production[†] and updates the previous DELPHI measurements on $\mathrm{K}^{*0}(892)$ production [13].

The data collected by the DELPHI experiment in 1994 were used for the study of $\mathrm{K}^{*0}(892)$, $\phi(1020)$ and $\mathrm{K}_2^{*0}(1430)$ production; during this running period the DELPHI Ring Imaging Cherenkov (RICH) detectors were fully operational, allowing good particle identification. The sample corresponds to a total of 1.3 million hadronic Z decays. The $\phi(1020)$ production was also studied with 2.9 million hadronic events collected by DELPHI in 1991-1994 without use of particle identification.

After a brief description of the DELPHI detector and the selection of hadronic Z decays, the charged particle identification procedure and the fitting procedures used to extract the $\mathrm{K}^{*0}(892)$, $\phi(1020)$ and $\mathrm{K}_2^{*0}(1430)$ signals from the $\mathrm{K}^{\pm}\pi^{\mp}$ and $\mathrm{K}^+\mathrm{K}^-$ invariant mass distributions are described. The production rates and their differential cross sections are then presented and compared with other measurements and with model expectations.

2 Experimental Procedure

2.1 Event and particle selection

Detailed descriptions of the DELPHI detector and its performance can be found elsewhere [14,15]. Here, only the specific properties relevant to the present analysis are summarized.

The charged particle tracks are measured in the 1.2 T magnetic field by a set of tracking detectors. The average momentum resolution for charged particles in hadronic

[†]Unless otherwise stated, antiparticles are implicitly included.

final states is in the range $\Delta p/p \simeq 0.001p$ to $0.01p$ (p in GeV/c), depending on which detectors are included in the track fit.

A charged particle is accepted in this analysis if it has momentum p greater than 0.2 GeV/c, momentum error $\Delta p < p$, polar angle θ with respect to the beam axis between 25° and 155°, measured track length in the Time Projection Chamber (TPC) greater than 50 cm, and impact parameter with respect to the nominal crossing point within 5 cm in the transverse (xy) plane and 10 cm along the beam direction (z-axis).

Hadronic events are then selected if there are at least 5 charged particles, if the total energy of charged particles (assumed to be pions) in each of two hemispheres (θ above and below 90°) exceeds 3 GeV, if the total energy of all charged particles is greater than 15 GeV, if the polar angle of the sphericity axis is between 40° and 140°, and if (when particle identification is used) the information from the RICH detectors is available for at least one charged particle. The contamination from events due to beam-gas scattering and to $\gamma\gamma$ interactions is estimated to be less than 0.1% and the background from $\tau^+\tau^-$ events to be less than 0.2% of the accepted events.

The samples of 846,627 and 1,852,000 events collected in 1994 and 1991-1994 respectively and selected with the above cuts will be referred to as the ones passing the standard cuts. After the event selection, in order to ensure a better signal-to-background ratio for the resonances in the $K^{\pm}\pi^{\mp}$ and K^+K^- invariant mass spectra, stronger restrictions on the track impact parameters with respect to the nominal crossing point were imposed: they had to be within 0.3 cm in the transverse plane and 2 cm along the beam direction. The samples selected with these additional cuts will be referred to as those passing the strong cuts.

Charged kaon identification in this analysis is provided by the RICH detectors. In these detectors, particle identification is based primarily on comparing the measured Cherenkov angle with that expected for each mass hypothesis. This is called the ring identification mode (for more details, see [15] and refs. therein). The raw photoelectron distributions were described as the sum of the expected Cherenkov signal and a flat background and their probabilities to come from π, K and proton were calculated. For particles below the Cherenkov threshold, $\beta < 1/n$, no light is emitted. This property is used in order to separate kaons and protons from pions in the momentum range from 2.5 to 9 GeV/c, where kaons and protons are below the threshold while pions and lighter particles emit photons. This is called the veto identification mode.

The RICH detectors enable identification of kaons of momentum above $\simeq$ 1 GeV/c. They rely on external tracking for the determination of the particle momentum and impact point. The Barrel RICH is placed between the TPC, the main tracking device of DELPHI, and another tracking detector, the Outer Detector (OD). For the veto mode of the RICH, requiring a track segment in the OD avoids particles which were scattered or lost due to an interaction in the RICH. It also improves the quality of the track extrapolation. This is especially important for the liquid radiator, where the centre of the Cherenkov ring is given by the impact point of the track. Therefore, after the event selection and when particle identification is requested, the track of the selected particle is required to be detected in the OD.

The identification performance was evaluated by means of the detector simulation program DELSIM [15]. In DELSIM, about 3.4 million events were generated using the JETSET program [3] with the DELPHI default parameters [5] obtained before the measurements reported in this paper (this version will be referred to below as tuned JETSET). The particles were followed through the detector and the simulated digitizations obtained

were processed with the same reconstruction programs as the experimental data. The efficiency of the kaon identification was found to be about 70% on average.

The $K^{\pm}\pi^{\mp}$ invariant mass distributions were studied in the $\cos\theta_h \leq 0$ region, where θ_h is the helicity angle of the kaon, i.e. its angle in the $K^{\pm}\pi^{\mp}$ rest frame with respect to the $K^{\pm}\pi^{\mp}$ line of flight. The kaon momentum range in this $\cos\theta_h$ region was almost completely covered by the liquid radiator. The main reason for selecting the $\cos\theta_h \leq 0$ region was to remove the low momentum pions. This avoided biases in the invariant mass distributions due to worse determination of the opening angle between $K^{\pm}$ and low momentum $\pi^{\mp}$. The removal of slow pions also reduced the influence of reflections from other meson resonances and of residual Bose-Einstein correlations resulting from interference of pions from the resonance decay with other pions in the jet (see sect. 2.2). For the K^+K^- invariant mass distributions, the full $\cos\theta_h$ region was used.

2.2 Treatment of detector imperfections and fit procedure

Particle identification inefficiencies as well as other detector imperfections, such as limited geometrical acceptance, particle interactions in the detector material, and the different kinematical cuts imposed for charged particle and event selection, were taken into account by applying the approach described in refs. [10,16] and outlined here.

In the present analysis, a vector $\vec{a}$ of parameters was used in the definition of the anticipated distribution function, $f(M,\vec{a})$, of the invariant mass M. The parameters $\vec{a}$ were then determined by a least squares fit of the function to the data.

For the $K^{\pm}\pi^{\mp}$ invariant mass distributions, this function was composed of three parts:

$$f(M,\vec{a}) = f^S(M,\vec{a}) + f^B(M,\vec{a}) + f^R(M,\vec{a}). \tag{1}$$

The function

$$f^S(M,\vec{a}) = a_1 W_V(M)\cdot BW_V(M,a_2,a_3) + a_4 W_T(M)\cdot BW_T(M,a_5,a_6) \tag{2}$$

described the $K^{*0}(892)$ and $K_2^{*0}(1430)$ resonance signals in the $K^{\pm}\pi^{\mp}$ invariant mass distributions. A background term was taken in the form:

$$f^B(M,\vec{a}) = a_7(M-M_{th})^{a_8}\cdot\exp(a_9 M + a_{10}M^2 + a_{11}M^3), \tag{3}$$

where M_{th} is the invariant mass threshold. The third term in eq. 1 represents a sum of the different reflection functions (RF_i):

$$f^R(M,\vec{a}) = \sum_{i\geq 12} a_i RF_i(M). \tag{4}$$

The two terms in eq. 2 represent the relativistic Breit–Wigner functions BW_V and BW_T for the $K^{*0}(892)$ and $K_2^{*0}(1430)$, respectively, multiplied by the functions $W_V(M)$ and $W_T(M)$ accounting for distortion of the resonance Breit–Wigner shapes by phase space effects and by residual Bose–Einstein (BE) correlations. As in [10], they were obtained by generating the invariant mass distribution for the resonance using the tuned JETSET program [5], where BE correlations were included. Then the generated distribution (with its integral normalized to one) was divided by the analytical Breit–Wigner function used in JETSET (with its integral also normalized to one).

If the influence of phase space and residual BE correlations was ignored completely ($W(M)=1$), then for the full measured range, $0.04 \leq x_p \leq 0.7$ ($x_p = p/p_{beam}$), the fitted $K^{*0}(892)$ mass, 893.5 $\pm$ 0.9 MeV/c^2, was shifted by -2.6 MeV/c^2 (i.e. by 3 standard

deviations) from the world average (PDG) of 896.1 $\pm$ 0.3 MeV/c^2 [17] and the measured $K^{*0}(892)$ cross section decreased by 2.5%. The same mass shift was observed when phase space effects were accounted for but BE effects were still ignored. The mass shift was in fact seen only in the smallest x_p-region, $0.04 \leq x_p \leq 0.1$, as expected for residual BE correlations. However, including BE correlations resulted in a fitted $K^{*0}(892)$ mass of 898.8 $\pm$ 0.8 MeV/c^2, larger than the PDG value by 2.7 MeV/c^2. The shift was again essentially due to the smallest x_p-region. Although this shows that the treatment of BE correlations in JETSET is not perfect, the JETSET ansatz was used. The uncertainty in treating BE correlations at small x_p values was accounted for in the systematic errors. The fits to the $K^{\pm}\pi^{\mp}$ invariant mass spectra were performed over a mass range from 0.64 to 2.0 GeV/c^2.

For the K^+K^- mass spectra in the $\phi(1020)$ mass region, the fits were made in the mass range from 0.988 to 1.1 GeV/c^2, with only the first Breit-Wigner term in eq. 2 and with only one term in the exponential in eq. 3.

Two types of reflection functions contributing to eq. 4 have been considered.

Reflections of the first type arise from imperfect particle identification when, for example, resonances in the $\pi^+\pi^-$ and K^+K^- systems distort the $K^{\pm}\pi^{\mp}$ mass spectra. The influence of most of these reflections is relatively small due to quite reliable kaon identification and the $\cos\theta_h \leq 0$ selection. The functions $RF_i(M)$ in eq. 4 were determined from events generated according to the tuned JETSET model [5]. Then contributions of the reflections to the uncorrected mass spectra defined by function $\bar{N}_m^R(\vec{a})$ (eq. 6 below) were obtained by passing these events through detector simulation. In this way the influence of particle misidentification was also properly accounted for. The reflection contributions to the uncorrected $K^{\pm}\pi^{\mp}$ mass spectra, $\bar{N}_m^R(\vec{a})$, defined in this way with the parameters a_i (with $i \geq 12$) in eq. 4 taken from JETSET are shown in Fig. 1. Subsequently the parameters a_i were redefined either from the fit or from the experimental cross sections measured by DELPHI and/or other LEP experiments [1].

Although reflections from many particles and resonances were considered, only the most important ones were finally taken into account. The largest contribution from the reflections of the first type strongly influencing the $K_2^{*0}(1430)$ cross section comes from the narrow $f_2'(1525)$ resonance (Fig. 1g). It was calculated using the $f_2'(1525)$ production rate measured by DELPHI [11].

Another type of distortion of the $K^{\pm}\pi^{\mp}$ mass spectra (also denoted for simplicity as RF_i in eq. 4) arises either from the resonances in the same system, such as $K_0^{*0}(1430) \rightarrow K^+\pi^-$[‡], or from charmed particle production. Charm meson production and decay distort significantly the invariant mass distributions in the tensor meson mass region. The influence of the D^0 is illustrated in Fig. 1i. It shows, apart from the sharp peak due to $D^0 \rightarrow K^-\pi^+$ decay, the presence of the relatively narrow peak at $M \simeq 1.6$ GeV/c^2 arising from the quasi-two-body $D^0 \rightarrow K^{*-}(892)\pi^+$ decay, when the π^+ from the D^0 decay and the K^- from the $K^{*-}(892)$ decay form the $K^-\pi^+$ system. As for the reflections of the first type, these distortions were also obtained from events generated by JETSET and passed through detector simulation.

Finally the reflections (not shown) from the η and η' in the K^+K^- mass spectrum in the $\phi(1020)$ meson mass region when particle identification was not used were found to be quite important for $x_p \leq 0.2$ and were accounted for in the same way. Their contributions were negligible when particle identification was used.

[‡] The influence of this broad $K_0^{*0}(1430)$ resonance on the $K_2^{*0}(1430)$ was found to be small.

In each mass bin, m, the number of entries $\bar{N}_m(\vec{a})$ predicted by the function $f(M,\vec{a})$ is given by:

$$\bar{N}_m(\vec{a}) = \bar{N}^S_m(\vec{a}) + \bar{N}^B_m(\vec{a}) + \bar{N}^R_m(\vec{a}), \tag{5}$$

where

$$\bar{N}^G_m(\vec{a}) = C^G_m \sum_n S^G_{mn} A^G_n f^G_n(\vec{a}), \tag{6}$$

$$f^G_n(\vec{a}) = \int_{M_n}^{M_{n+1}} f^G(M,\vec{a}) dM \tag{7}$$

where $G = S, B$ or R and M_n is the lower edge of the n-th histogram bin of the variable M. The coefficients A_n characterize the detector acceptance and C_m the losses of particles due to the selection criteria imposed and the extra particles due to ghosts, secondary interactions etc. The smearing matrix S_{mn} is determined by the experimental resolution (see [10] for more details). The three terms in eq. 5 are necessary because the resonance signals, for example in the $\mathrm{K}^{\pm}\pi^{\mp}$ invariant mass distribution, contain by definition only the $\mathrm{K}^{\pm}\pi^{\mp}$ pairs, while the background is contaminated by the misidentified $\pi^+\pi^-$, $\mathrm{K}^+\mathrm{K}^-$, $\mathrm{K}^{\pm}\mathrm{p}^{\mp}$ and $\mathrm{p}^{\pm}\pi^{\mp}$ pairs. Therefore the coefficients, C_m, for the resonance signals and for the background are expected to be different (see [16] for more details).

The best values for $\vec{a}$ were then determined by a least squares fit of the predictions of eq. 5 to the measured values, N_m, by minimizing the function:

$$\chi^2 = \sum_m (N_m - \bar{N}_m(\vec{a}))^2/\sigma^2_m + \sum_i (a_i - \bar{a}_i)^2/(\Delta\bar{a}_i)^2, \tag{8}$$

where $\sigma^2_m = N_m + \sigma^2(\bar{N}_m)$ and $\sigma(\bar{N}_m)$ is the error of $\bar{N}_m$ (which is much less than $\sqrt{N}_m$) due to the finite statistics of the simulation used to evaluate A_n, C_m and S_{mn}. The second sum in eq. 8 constrains appropriate resonance properties to the values $\bar{a}_i \pm \Delta\bar{a}_i$ taken from external sources. In particular, the variations within errors of a) the particle production rates taken from other experiments to determine the normalization of the reflection functions and b) the masses and widths taken from the PDG tables [17] were both accounted for by the second term of eq. 8. Thus the "statistical" errors obtained from the fits include a systematic component.

The vector (V) and tensor (T) meson production rates were calculated as

$$\langle N \rangle = \frac{1}{\mathrm{BR}} \frac{1}{\langle R \rangle} \int f^S_{V(T)}(M,\vec{a})\ dM, \tag{9}$$

where the factor 1/BR takes into account the unobserved decay modes and the integration limits are the same as the fit ranges. The meaning of $\langle R \rangle$ is explained below.

The "standard" event and particle selection cuts were chosen to ensure that the average charged particle multiplicity for the data and simulated events were the same. Due to the detector simulation imperfections, this is not necessarily the case when the stronger cuts on impact parameters are applied. Indeed, the ratios of the $\mathrm{K}^{\pm}\pi^{\mp}$ ($\mathrm{K}^+\mathrm{K}^-$) invariant mass distributions, $\mathrm{d}\sigma/\mathrm{d}M$, obtained for the samples with the standard and stronger cuts are different for the data events ($R_D = \mathrm{d}\sigma_{standard}/\mathrm{d}\sigma_{strong}$) and the simulated events (R_S). To take this into account, the production rates were divided by the average values of the factor $R = R_S(M)/R_D(M)$ in each of the x_p-intervals considered. These factors R together with their average values $\langle R \rangle$ are shown for the $\mathrm{K}^{\pm}\pi^{\mp}$ mass spectra in Fig. 2 for several x_p-intervals. The dependence of R on M is small in all x_p-intervals, but larger deviations from unity are seen for small x_p values than for large ones. The errors of $\langle R \rangle$ in Fig. 2 take into account the statistical fluctuations of R and its deviation from being constant in the mass range considered. The statistical fluctuations are absorbed into the

statistical errors of the production rates while any deviation from a constant, together with the variations of $\langle R \rangle$ with the different selection criteria imposed, are accounted for in the systematic errors. The total uncertainties in the coefficient $\langle R \rangle$ are below $\pm 4\%$.

The reliability of the fit procedure was verified with the simulated events. The simulated $K^{\pm}\pi^{\mp}$ (K^+K^-) invariant mass distributions in different x_p-intervals were fitted applying the formulae (1)–(8), but with the non-relativistic resonance Breit–Wigner shapes used in JETSET. The fit described the uncorrected data after detector simulation very well. The resonance x_p-spectra (not shown) and the corresponding average multiplicities per hadronic Z decay in the indicated x_p-ranges as given in Table 1 agreed within errors with those in JETSET tuned to the DELPHI data [5] and used in detector simulation. It should be stressed that no such agreement was achieved without treatment of the reflections described above, especially for the $K_2^{*0}(1430)$ produced with relatively small cross section.

Table 1: The average multiplicities per hadronic Z decay for the $K^{*0}(892)$, $\phi(1020)$ and $K_2^{*0}(1430)$ in the indicated x_p-ranges obtained from the fits to the uncorrected simulated events after DELSIM in comparison with the corresponding values as generated by the tuned JETSET at the input to DELSIM. The errors are statistical (resulting from the fits).

Resonance	x_p-range	Fit Results	JETSET (tuned)
$K^{*0}(892)$	0.04–0.7	0.592 ± 0.009	0.586
$\phi(1020)$	0.05–1.0	0.071 ± 0.002	0.071
$K_2^{*0}(1430)$	0.04–0.7	0.132 ± 0.013	0.131

3 Results and Discussion

3.1 $K^{*0}(892)$ production

The measured uncorrected $K^{\pm}\pi^{\mp}$ invariant mass distributions are shown for the individual x_p-intervals in Fig. 3 together with the results of the fits. In the fits, the $K^{*0}(892)$ width and the $K_2^{*0}(1430)$ mass and width were constrained by the second term in eq. 8 and the $K^{*0}(892)$ mass was left free to take into account its small shift. The fits describe the data quite well in all x_p-intervals. The $K^{*0}(892)$ differential production cross section, $(1/\sigma_h)\cdot d\sigma/dx_p$ where σ_h is the total hadronic cross section, is presented in Table 2 and in Fig. 4.

The measured average $K^{*0}(892)$ multiplicity per hadronic event in the $0.04 \leq x_p \leq 0.7$ range obtained by integrating the x_p-spectrum was determined to be:

$$\langle K^{*0}(892) \rangle \ = 0.570 \pm 0.016(stat), \tag{10}$$

where the error is the statistical one obtained from the fit. It agrees with the corresponding value of 0.567 ± 0.015(stat) obtained by fitting the overall mass spectrum in the $0.04 \leq x_p \leq 0.7$ range.

The systematic errors were estimated by analyzing the contributions arising from:

1. choice of the background parameterization, bin size of the mass spectra, and mass range used in the fit;

Table 2: Differential $K^{*0}(892)$ cross sections $(1/\sigma_h)\cdot d\sigma/dx_p$ for $0.04 \leq x_p \leq 0.7$. The statistical and systematic errors are combined quadratically. The corresponding values of χ^2/NDF for the fits are also given.

x_p interval	$(1/\sigma_h)\cdot d\sigma/dx_p$	χ^2/NDF
0.04–0.06	4.67 $\pm$0.60	78/59
0.06–0.08	3.66 $\pm$0.41	60/59
0.08–0.10	2.74 $\pm$0.32	49/59
0.10–0.14	2.42 $\pm$0.24	77/59
0.14–0.18	1.43 $\pm$0.16	47/59
0.18–0.25	1.04 $\pm$0.10	48/59
0.25–0.35	0.64 $\pm$0.06	73/59
0.35–0.45	0.31 $\pm$0.04	48/59
0.45–0.70	0.11 $\pm$0.01	66/59

2. $K^{\pm}$ identification efficiency;
3. treatment of residual BE correlations;
4. variation of cuts imposed for the charged particle selections;
5. variation in absolute value of the factor $\langle R \rangle$.

The first contribution was found to be small, as could be expected from the good agreement of the results obtained from the fits to the simulated data with the input JETSET production rates (Table 1). Its total relative contribution of $\pm$2.7% was dominated by the uncertainty in the background parameterization.

The contribution from the uncertainty in the kaon identification efficiency was estimated to be about $\pm$6.0%.

The uncertainty in treatment of residual BE correlations (see sect. 2.2) gave a total relative error of $\pm$2.5%. Its strong x_p-dependence was taken into account.

The uncertainty arising from varying the particle selection was estimated by comparing the results obtained for the samples selected with the strong cuts, with the standard cuts, and with the cuts on the intersection point for each pair of oppositely charged particles described in [10]. Additional tests were performed to check the sensitivity of the results to other changes in the selection criteria: $K^{\pm}\pi^{\mp}$ pairs were selected only when both particles had hits in the vertex detector (VD), the tighter cuts on kaon identification criteria were applied, and different $\cos\theta_h$ regions were tried. The corresponding variations, including the uncertainty in the coefficient $\langle R \rangle$ accounting for imperfections in the simulation (which also varied depending on the selection criteria imposed) gave a $\pm$5.7% contribution to the total relative systematic error of $\pm$9.1%.

The measured production rate (10) was extrapolated to the full x_p range by normalizing the expectations of tuned JETSET in the $0.04 \leq x_p \leq 0.7$ range to the measured $K^{*0}(892)$ rate in this x_p-interval and taking the overall $K^{*0}(892)$ rate in the full x_p-range from the corresponding JETSET predictions. Good agreement in the small x_p-region (Fig. 4) between the measured x_p-spectrum and that predicted by tuned JETSET allowed the extrapolation error to be taken as $\pm$10% of the difference between values (11) and (10). This gave:

$$\langle K^{*0}(892) \rangle = 0.77 \pm 0.02(stat) \pm 0.07(syst) \pm 0.02(extr). \qquad (11)$$

This value agrees within errors with our previous measurement [13], but represents a significant improvement in precision. It is also consistent within errors with the recent OPAL [12] and ALEPH [18] results of 0.74 ± 0.04 and 0.83 ± 0.09 respectively.

The overall $K^{*\pm}(892)$ production rate per hadronic Z decay measured by OPAL [19] and DELPHI [10] amounted to 0.72 ± 0.08 and 0.712 ± 0.067 respectively. Thus the $K^{*0}(892)$ and $K^{*\pm}(892)$ are produced with approximately equal probabilities, as could be expected. Fig. 4 shows that their differential production cross sections $(1/\sigma_h)\cdot d\sigma/dx_p$ are also approximately the same. It also shows the predictions for the $K^{*0}(892)$ of the tuned JETSET [5]. These are in reasonable agreement with the data, although the model predicts slightly harder fragmentation than is measured. The fragmentation function predicted by HERWIG 5.8 [4] (with default parameters) is in reasonable agreement with the data for $x_p \leq 0.4$ (Fig. 4), but is harder for $x_p \geq 0.4$. The overall $K^{*0}(892)$ production rates in HERWIG and tuned JETSET are equal to 0.806 and 0.794 respectively and agree with the measured value (11).

3.2 $\phi(1020)$ production

The narrow width of the $\phi(1020)$ allows a clear signal to be extracted even without kaon identification. Therefore the $\phi(1020)$ inclusive production can be measured either using particle identification in the RICH detector, as was done for the $K^{*0}(892)$, or assuming all charged particles to be kaons. The advantage of the method with kaon identification is the large signal-to-background ratio. On the other hand, the much smaller signal-to-background ratio in the method without particle identification can be partially compensated by the use of the full DELPHI statistics accumulated in 1991-1994 with almost 2 million hadronic events selected after the standard cuts. Besides, the analysis of the results obtained a) with both K^+ and K^- identified, b) with at least one identified kaon, and c) ignoring identification allows a check on the efficiency of the identification and better understanding of the possible systematics. For these reasons, all three methods were used.

The measured uncorrected K^+K^- invariant mass distributions for the 1991-1994 data obtained without particle identification are presented for the individual x_p-intervals in Fig. 5. The corresponding mass distributions for the 1994 data with at least one kaon or both kaons required to be identified by the RICH detector are presented in Fig. 6 and Fig. 7 respectively. Fig. 5 shows that the $\phi(1020)$ signal is seen even without particle identification in all x_p-intervals. The combinatorial background dominated by misidentified pions is very large at small x_p. However, it decreases significantly with increasing x_p, so that the signal to background ratio becomes reasonable for $x_p \geq 0.2$. Requiring identification of at least one kaon by the RICH reduces the background significantly for all x_p values, but the statistical significance of the $\phi(1020)$ signal becomes small for $x_p \geq 0.5$ (Fig. 6). With both kaons identified by the RICH, the large $\phi(1020)$ signals are well seen over the small background, but the statistics are poor for large x_p (Fig. 7).

In the fits, for all three cases, the $\phi(1020)$ mass and width were constrained by the second term in eq. 8. It should be stressed that the limited mass resolution, which in the case of the $\phi(1020)$ is comparable to its width and thus influences the signal significantly, is taken into account in the applied method by the smearing matrix S_{mn} (see Eq. 6). The fits describe the data in Figs. 5 - 7 quite well in all x_p-intervals.

Table 3 compares the $\phi(1020)$ differential cross sections in the $0.05 \leq x_p \leq 0.5$ range obtained with both kaons identified, at least one kaon identified, and without identification. For this, the same data sample collected in 1994 was used. In the $0.1 \leq x_p \leq 0.5$

range, the results agree quite well. This shows that the kaon identification efficiencies are correctly reproduced by detector simulation in this x_p-range. However, the important differences in the results in the first $0.05 \leq x_p \leq 0.1$ interval might indicate some problems with the treatment of the identification efficiencies at the smallest x_p values.

Table 3: Differential $\phi(1020)$ cross sections $(1/\sigma_h)\cdot \mathrm{d}\sigma/\mathrm{d}x_p$ for $0.05 \leq x_p \leq 0.5$ obtained with a) both kaons identified, b) at least one kaon identified, and c) without requiring kaon identification. The errors are the statistical ones obtained from the fit. The corresponding χ^2/NDF values for the fits are also given.

	K^+ and K^- identified		At least one K identified		No identification	
x_p-interval	$(1/\sigma_h)\cdot \mathrm{d}\sigma/\mathrm{d}x_p$	χ^2/NDF	$(1/\sigma_h)\cdot \mathrm{d}\sigma/\mathrm{d}x_p$	χ^2/NDF	$(1/\sigma_h)\cdot \mathrm{d}\sigma/\mathrm{d}x_p$	χ^2/NDF
0.05–0.10	0.357±0.028	56/52	0.436±0.024	52/52	0.373±0.039	13/16
0.10–0.15	0.278±0.024	63/52	0.261±0.019	75/52	0.280±0.026	13/16
0.15–0.20	0.212±0.020	47/52	0.181±0.014	53/52	0.206±0.020	16/16
0.20–0.30	0.131±0.012	54/52	0.123±0.009	65/52	0.159±0.012	17/16
0.30–0.50	0.057±0.008	52/52	0.063±0.005	58/52	0.075±0.007	21/16

For $0.05 \leq x_p \leq 0.2$, the resulting $\phi(1020)$ differential cross section was taken by averaging the results obtained with both identified kaons and with at least one identified kaon as given in the first three x_p-intervals of Table 3. Half of the difference between these values was attributed to the systematic error. For $0.2 \leq x_p \leq 1$, the results obtained without particle identification based on the 1991-1994 data sample were used. The differential cross section thus obtained is presented in Table 4 and in Fig. 4.

Table 4: Differential $\phi(1020)$ cross sections $(1/\sigma_h)\cdot \mathrm{d}\sigma/\mathrm{d}x_p$ for $0.05 \leq x_p \leq 1$. The statistical and systematic errors are combined quadratically.

x_p-interval	$(1/\sigma_h)\cdot \mathrm{d}\sigma/\mathrm{d}x_p$
0.05 – 0.10	0.396 ± 0.055
0.10 – 0.15	0.269 ± 0.030
0.15 – 0.20	0.197 ± 0.027
0.20 – 0.25	0.186 ± 0.017
0.25 – 0.30	0.134 ± 0.014
0.3–0.4	0.104 ± 0.010
0.4–0.5	0.047 ± 0.006
0.5–0.7	0.022 ± 0.003
0.7–1.0	0.0040± 0.0007

The measured average $\phi(1020)$ multiplicity per hadronic event for $0.05 \leq x_p \leq 1$ obtained by integrating the x_p-spectrum was determined to be:

$$\langle \phi(1020) \rangle \ = 0.080 \pm 0.002(stat) \pm 0.005(syst). \qquad (12)$$

In calculating the systematic errors, the possible influence of residual Bose-Einstein correlations was ignored, since the probability to have another $K^{\pm}$ close to the $\phi(1020)$ decay products in phase space is small. The uncertainties due to η and η' reflections for

$0.05 \leq x_p \leq 0.2$ when particle identification was used and for $x_p \geq 0.2$ without use of particle identification were found to be negligible. The uncertainties arising from the particle selection, including the uncertainty in the coefficient $\langle R \rangle$ accounting for imperfections in the simulations resulted, as in case of the $K^{*0}(892)$, in a relative error of $\pm 5.7\%$. This relative error was taken into account in (12) and in each of the x_p-intervals. Besides, half of the difference between the results obtained with both identified kaons and with at least one identified kaon (see Table 3) was taken as a systematic uncertainty in all of the x_p-intervals lying in the range $0.05 \leq x_p \leq 0.2$. In the same x_p-intervals, an additional error of $\pm 4\%$ was assigned due to the uncertainty in the kaon identification efficiency. The resulting total relative systematic error in (12) amounts to $\pm 6.3\%$.

The measured production rate (12) was extrapolated to the full x_p range by normalizing the expectations of the tuned JETSET in the $x_p \geq 0.05$ range to the measured $\phi(1020)$ rate in this x_p-interval and taking the overall $\phi(1020)$ rate in the full x_p-range from the corresponding JETSET prediction. The uncertainty in this procedure is accounted for as for the $K^{*0}(892)$. This gives:

$$\langle \phi(1020) \rangle \ = 0.104 \pm 0.003(stat) \pm 0.007(syst) \pm 0.002(extr). \qquad (13)$$

Compatible results were obtained without use of particle identification in the measured x_p-range.

The overall $\phi(1020)$ production rate agrees within errors with the prediction, 0.093, of the tuned JETSET (tuned before this measurement) and is only slightly smaller than the HERWIG prediction of 0.122. The $\phi(1020)$ differential production cross section $(1/\sigma_h) \cdot d\sigma/dx_p$ (Fig. 4) is reproduced by the tuned JETSET reasonably well. HERWIG, as in the case of the $K^{*0}(892)$, agrees with the data for $x_p \leq 0.4$, but predicts a much harder fragmentation in the large x_p-region than the data exhibit. The value (13) can be compared with the recent OPAL [12] and ALEPH [18] measurements of 0.100 ± 0.008 and 0.122 ± 0.009 respectively.

3.3 $K_2^{*0}(1430)$ production

The overall $K_2^{*0}(1430)$ tensor meson production rate of 0.168 as predicted by the tuned JETSET is quite large. Therefore it was expected that the $K_2^{*0}(1430)$ signal could be easily detected. A study based on simulation showed a good agreement between the $K_2^{*0}(1430)$ rate found in the fit in the range $0.04 \leq x_p \leq 0.7$ and the JETSET value (Table 1). In the data, selected with the same cuts as for the $K^{*0}(892)$, only a rather small $K_2^{*0}(1430)$ signal was observed. Therefore additional selection criteria were tried in an attempt to improve the signal-to-background ratio. Only tracks with hits in the vertex detector were used, more stringent selection criteria on kaon identification were applied, the particles satisfying cuts on kaon and proton selections were removed from the pion sample. However, these additional selection criteria had little influence on the magnitude of the $K_2^{*0}(1430)$ signal. The $K_2^{*0}(1430)$ signal in the measured uncorrected $K^{\pm}\pi^{\mp}$ invariant mass distribution for $0.04 \leq x_p \leq 0.7$ shown in Fig. 8a corresponds to a production rate of

$$\langle K_2^{*0}(1430) \rangle \ = 0.065 \pm 0.021(stat). \qquad (14)$$

Attempts to decrease the combinatorial background by cuts on the charged particle multiplicities $n_{ch} \leq 25$ or by subtracting bin by bin the histograms for like charged combinations did not change this result. It should also be stressed that the $K^{*0}(892)$ production rate obtained with similar selection criteria remained the same as in (11), within statistical errors. At higher $K^{\pm}\pi^{\mp}$ masses, the reflections from the quasi-two-body and two-body

D^0 decays in Fig. 8a are well reproduced. Moreover, a fit with the contribution of the D^0 reflection set free resulted in an overall D^0 production rate of $0.38\pm$ 0.05(stat), compatible within errors with the published LEP value of 0.40 ± 0.06 [17]. All this reinforces our confidence in the result obtained.

The systematic error was calculated taking into account the same sources of systematic uncertainties as for the $K^{*0}(892)$. An important contribution came from the variation in the results obtained with different track selections. Another important contribution was the uncertainty in the $f_2^{'}(1525)$ reflection (this appears as a contribution to the statistical error, see sect. 2.2). This was estimated using the $f_2^{'}(1525)$ production rate given in [11]. Disregarding the $f_2^{'}(1525)$ reflection would have resulted in a 1.5 times higher $K_2^{*0}(1430)$ rate.

The smallness of the signal did not allow measurement of the $K_2^{*0}(1430)$ x_p-spectrum to check if it was consistent in shape with the model expectations. Therefore the extrapolation of the measured production rate (14) to the full x_p-region must be treated with caution. Nevertheless, if such an extrapolation is made applying the procedure used for the $K^{*0}(892)$ and $\phi(1020)$ but this time assuming a $\pm 50\%$ extrapolation error, it results in:

$$\langle K_2^{*0}(1430)\rangle \ = 0.079 \pm 0.026(stat) \pm 0.030(syst) \pm 0.007(extr) \qquad (15)$$

and

$$\langle K_2^{*0}(1430)\rangle / \langle K^{*0}(892)\rangle = 0.10 \pm 0.05. \qquad (16)$$

The value (15) can be compared with the previous DELPHI estimate of the $K_2^{*\pm}(1430)$ production rate of $0.05^{+0.07}_{-0.05}$ [10]. They agree within large errors. On the other hand, the value (15) is 2.4 times smaller than the corresponding value of $0.19 \pm 0.04 \pm 0.06$ for $x_E \leq 0.3$ measured by OPAL [12], although compatible within 1.35 standard deviations. The predictions of the tuned JETSET, 0.168, and of HERWIG, 0.137, are also much larger than the value (15).

As was mentioned earlier, the $K_2^{*0}(1430)$ production rate obtained from the fit to the generated data after detector simulation reproduced the JETSET prediction well at the input to the simulation (Table 1). Fig. 8b illustrates the results of such a fit. Comparing Figs. 8a and 8b shows that if the $K_2^{*0}(1430)$ signal was indeed as large in the data as in JETSET it would certainly be detected.

The $\langle K_2^{*0}(1430)\rangle / \langle K^{*0}(892)\rangle$ ratio (16) appears to be smaller than the measured ratios [10,11]:

$$\langle f_2(1270)\rangle / \langle \rho^0(770)\rangle = 0.24 \pm 0.07 \qquad (17)$$

and

$$\langle f_2^{'}(1525)\rangle / \langle \phi(1020)\rangle = 0.19 \pm 0.07, \qquad (18)$$

although the errors are quite large. It would be difficult to accommodate this difference into the present versions of the JETSET and HERWIG models.

But is this difference surprising? It is true, as noticed in [13], that the $\langle K_2^{*0}(1430)\rangle / \langle K^{*0}(892)\rangle$ and $\langle f_2(1270)\rangle / \langle \rho^0(770)\rangle$ ratios in hadronic reactions were found to be the same. However, the $\langle K_2^{*0}(1430)\rangle / \langle K^{*0}(892)\rangle$ ratio was measured mainly in kaon induced reactions [20]-[24]. As stressed in the same papers [20]-[24], the inclusive production of $K^*(892)$ and $K_2^*(1430)$ in these reactions was strongly dominated by the fragmentation of the strange valence s-quark in the incident kaon. In the high x region ($x = 2p_L/\sqrt{s}$) the $\langle K_2^{*0}(1430)\rangle / \langle K^{*0}(892)\rangle$ ratio was higher than average, approaching unity as $x \to 1$, as also happened for the $\langle f_2(1270)\rangle / \langle \rho^0(770)\rangle$ [10] and $\langle f_2^{'}(1525)\rangle / \langle \phi(1020)\rangle$ [11] ratios for $x_p \to 1$ in e^+e^- annihilations. On the other hand, in the $x \leq 0$ region, the $\langle K_2^{*0}(1430)\rangle / \langle K^{*0}(892)\rangle$ ratio was below the average. This suggests that the relative

amount of the $K_2^*(1430)$ and $K^*(892)$ mesons produced from the sea quarks, the dominant production mechanism in e^+e^- annihilations as well as in pp or πp reactions, is much smaller. These arguments are supported by the the lack of evidence for important $K_2^*(1430)$ production in pp and πp reactions. For example, in the pp experiment at 400 GeV/c [25], where inclusive $\rho^0(770)$, $K^*(892)$ and $f_2(1270)$ production was measured quite precisely, no evidence for the $K_2^*(1430)$ was seen. In pp reactions at the higher ISR energies of $\sqrt{s}$ = 53 GeV, where the $K_2^{*0}(1430)$ production was measured [26,27], the situation is quite contradictory. The measured $\langle K_2^{*0}(1430)\rangle/\langle K^{*0}(892)\rangle$ ratio, 0.23 $\pm$ 0.08, in [27] is larger than the DELPHI value (16) and consistent with the DELPHI values (17) and (18). However, the measured $K_2^{*0}(1430)$ rate in [26] is by an order of magnitude smaller than in [27].

It can be also noticed that the thermodynamical model [8,28], which agrees with LEP results on the pseudoscalar and vector meson production rates, predicts $\langle K_2^{*0}(1430)\rangle$ = 0.049 and $\langle K_2^{*0}(1430)\rangle/\langle K^{*0}(892)\rangle$ = 0.071 in agreement with the DELPHI values (15) and (16). The model of ref. [9] predicts $\langle K_2^{*0}(1430)\rangle$ = 0.102 and $\langle K_2^{*0}(1430)\rangle/\langle K^{*0}(892)\rangle$ = 0.10, also in agreement with the DELPHI values.

4 Summary

The production of $K^{*0}(892)$, $\phi(1020)$ and $K_2^{*0}(1430)$ mesons has been measured by DELPHI in hadronic Z decays at LEP. The following conclusions can be drawn.

- The measured overall $K^{*0}(892)$ production rate per hadronic Z decay, 0.77 $\pm$ 0.08 and its x_p-spectrum are in good agreement with those for the $K^{*\pm}(892)$ meson [10] and with the tuned JETSET [5]. HERWIG 5.8 agrees reasonably with the data for small x_p, but predicts harder fragmentation for large x_p than the data exhibit.
- The measured overall $\phi(1020)$ production rate per hadronic Z decay, 0.104 $\pm$ 0.008, and its x_p-spectrum are in reasonable agreement with the tuned JETSET. As for the $K^{*0}(892)$, HERWIG agrees with the data for small x_p, but predicts harder fragmentation for large x_p than the data exhibit.
- The $K_2^{*0}(1430)$ production rate per hadronic Z decay, 0.079 $\pm$ 0.040, agrees with the $K_2^{*\pm}(1430)$ production rate, $0.05^{+0.07}_{-0.05}$, previously measured by DELPHI [10]. This $K_2^{*0}(1430)$ production rate is 2.4 times smaller than that measured by OPAL [12], although the two values are compatible within 1.35 standard deviations. It is significantly lower than predicted by the tuned JETSET and HERWIG, but agrees with the thermodynamical model prediction [8,28] and with the prediction of [9].

Apart from the $a_2(1320)$ resonance, all other members of the SU(3) tensor meson nonet have been measured by LEP experiments. Tensor meson production was found to be quite important. The most interesting result of this study is the important difference between the $K_2^{*0}(1430)$ and $f_2(1270)$ production rates, and between $\langle K_2^{*0}(1430)\rangle/\langle K^{*0}(892)\rangle$ and $\langle f_2(1270)\rangle/\langle \rho^0(770)\rangle$ or $\langle f_2^{'}(1525)\rangle/\langle \phi(1020)\rangle$ production rate ratios.

These results show that still more efforts are needed to improve the precision on the tensor meson production rates already measured and, in particular, to measure the $a_2(1320)$ production rate. The latter is important for understanding the mass dependence of the tensor meson production rates and its relation to the regularities observed for the pseudoscalar and vector meson nonets and the baryon octet and decuplet [6]. For this, the combined effort of all LEP experiments with the total statistics accumulated at LEP 1 is necessary.

Acknowledgements

We are greatly indebted to our technical collaborators and to the funding agencies for their support in building and operating the DELPHI detector, and to the members of the CERN-SL Division for the excellent performance of the LEP collider.

References

[1] A. De Angelis, *Light Quark Hadrons in Hadronic Z Decays*, PPE/95-135 (1995) and Proc. "EPS-HEP" 1995 Conference, Brussels (to be published).
[2] P.V. Chliapnikov, *Experimental Regularities in Particle Production Rates and in Multiplicity Distributions for e^+e^- Annihilations and $p^{\pm}p$ Collisions*, Proc. XXV Int. Symp. on Multiparticle Dynamics, Stara Lesna, Slovakia (1995) (to be published).
[3] T. Sjöstrand, Comp. Phys. Comm. **82** (1994) 74; CERN-TH. 7112/93 (1993, revised August 1994).
[4] G. Marchesini et al., Comp. Phys. Comm. **67** (1992) 465.
[5] DELPHI Collab., K. Hamacher et al, *Tuning and Test of Fragmentation Models Based on Identified Particles and Precision Event Shape Data*, paper eps0548 submitted to the "EPS-HEP" 1995 Conference, Brussels, and paper in preparation to be submitted to Z. Phys. C.
[6] P.V. Chliapnikov and V.A. Uvarov, Phys. Lett. **B345** (1995) 313.
[7] M. Szczekowski, Phys. Lett. **B357** (1995) 387.
[8] F. Becattini, Z. Phys. **C69** (1996) 485.
[9] Yi-Jin Pei, *Simple Approach to Describe Hadron Production Rates in e^+e^- Annihilation*, CERN-PPE/96-37, subm. to Z. Phys. **C**.
[10] DELPHI Collab., P. Abreu et al., Z. Phys. **C65** (1995) 587.
[11] DELPHI Collab., P. Abreu et al., *First Measurement of $f_2'(1525)$ Production in Z^0 Hadronic Decays* , PPE/96-26, to be published in Phys. Lett. B.
[12] OPAL Collab., R. Akers et al., Z. Phys. **C68** (1995) 1.
[13] DELPHI Collab., P. Abreu et al., Phys. Lett. **B298** (1993) 236.
[14] DELPHI Collab., P. Aarnio et al., Nucl. Instr. Meth. **A303** (1991) 233.
[15] DELPHI Collab., P. Abreu et al., *Performance of the DELPHI Detector,* PPE/95-194, to be published in Nucl. Instr. Meth. **A**.
[16] DELPHI Collab., P. Abreu et al., Phys. Lett. **B361** (1995) 207.
[17] Particle Data Group, L. Montanet et al., Phys. Rev., **D50** (1994) 1173.
[18] ALEPH Collab., D. Buskulic et al., Z. Phys. **C69** (1996) 379.
[19] OPAL Collab., P.D. Acton et al., Phys. Lett. **B305** (1993) 407.
[20] Mirabelle Collab., P.V. Chliapnikov et al., Z. Phys. **C12** (1982) 13.
[21] Mirabelle Collab., I.V. Ajinenko et al., Z. Phys. **C25** (1984) 103.
[22] Mirabelle Collab., Yu.I. Arestov et al., Z. Phys. **C6** (1979) 101; ibid. **C8** (1981) 283.
[23] BEBC Collab., M. Barth et al., Nucl. Phys. **B223** (1983) 267.
[24] EHS-NA22 Collab., N.M. Agababyan et al., Z. Phys. **C41** (1989) 539.
[25] LEBC-EHS Collab., M. Aguilar-Benitez et al., Z. Phys. **C50** (1991) 405.
[26] ARCCME Collab., A. Bohm et al., Phys. Rev. Lett. **41** (1978) 1761.
[27] ACCDHW Collab., D. Drijard et al., Z. Phys. **C9** (1981) 293.
[28] F. Becattini, private communication.

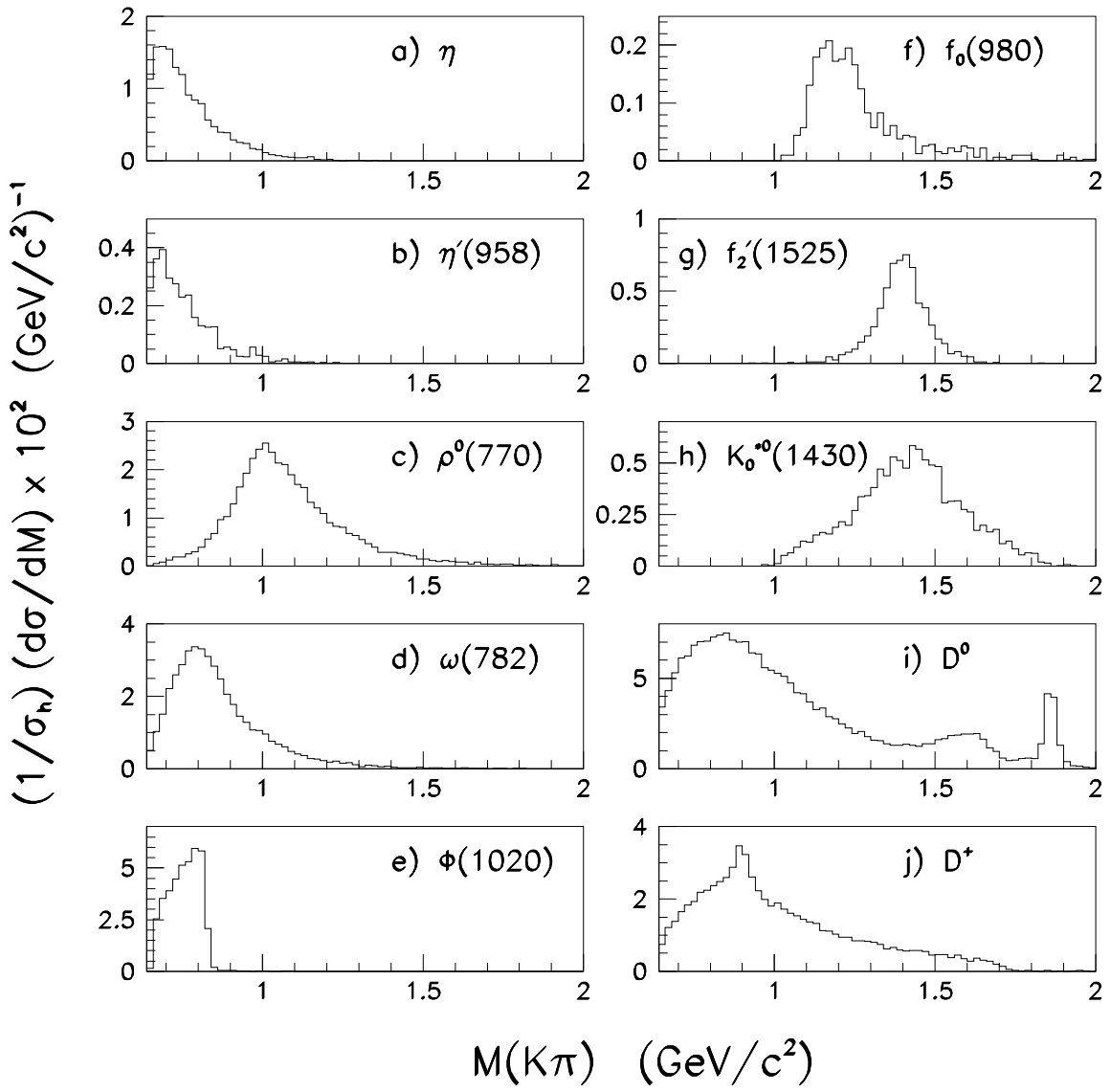

Figure 1: The reflection functions $\bar{N}^R(M,\vec{a})$ from the η, η', ρ^0, ω, ϕ, $f_0(980)$, $f_2'(1525)$, $K_0^{*0}(1430)$, D^0 and D^+ contributing to the uncorrected $K^{\pm}\pi^{\mp}$ invariant mass distribution for $0.04 \leq x_p \leq 0.7$ as taken from detector simulation.

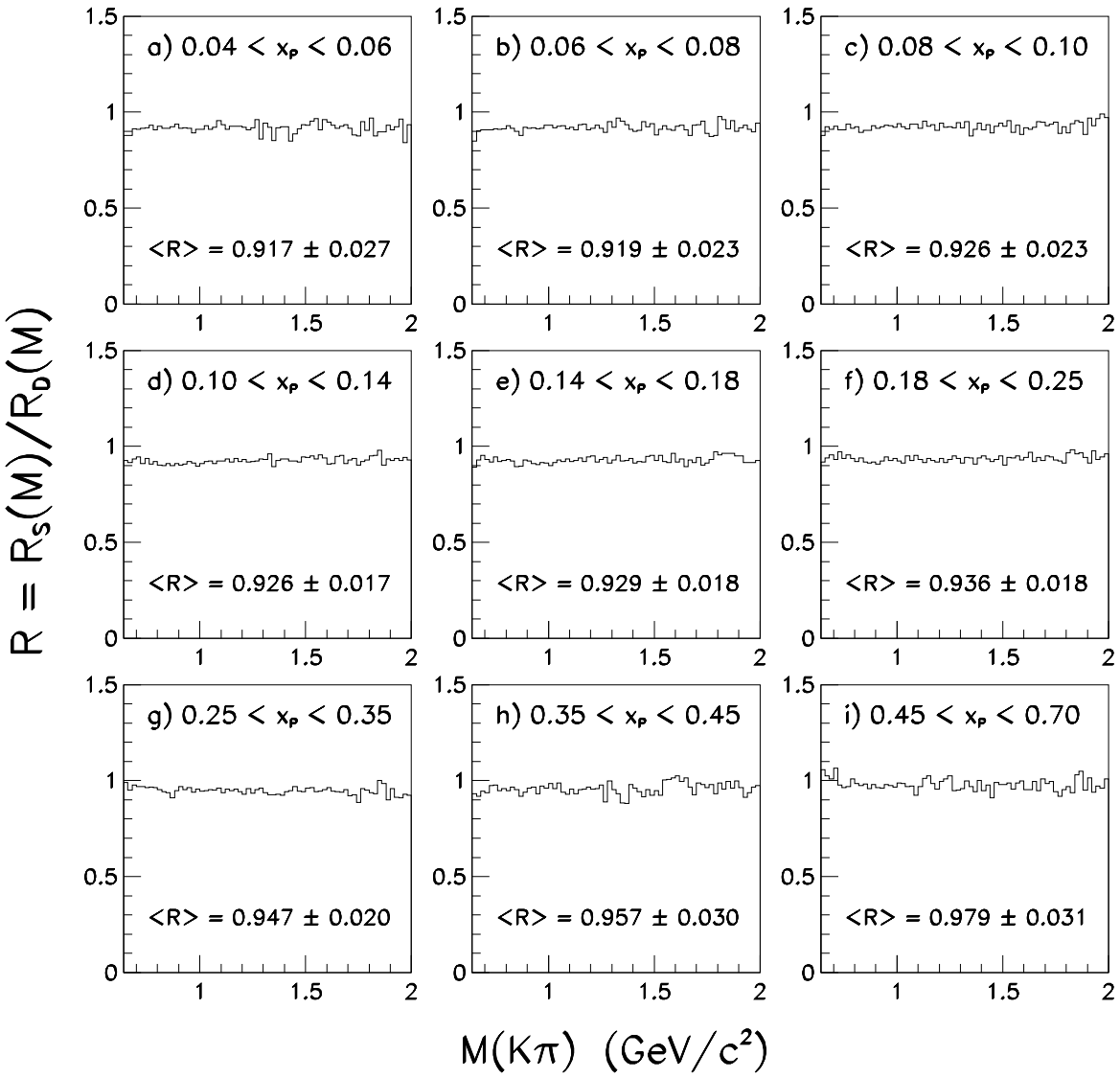

Figure 2: The coefficients $R(M) = R_S(M)/R_D(M)$ as a function of the $K^{\pm}\pi^{\mp}$ invariant mass for the indicated x_p-intervals. The values of R averaged over the full mass region in each x_p-interval are also given.

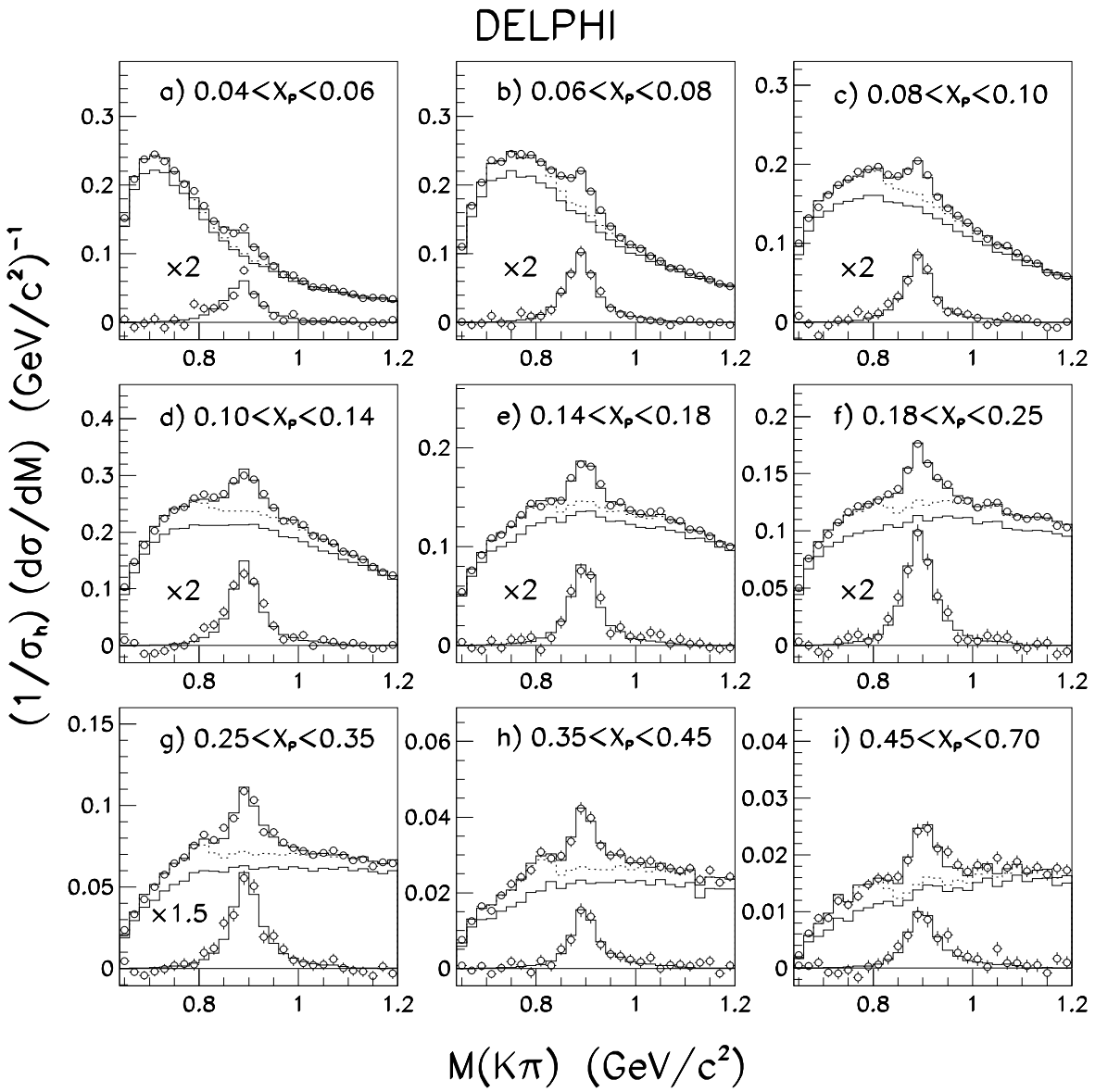

Figure 3: The $K^{\pm}\pi^{\mp}$ invariant mass spectra for the indicated x_p-intervals for the uncorrected data (open points). The upper solid histograms are the results of the fit. The background is shown by the lower solid histograms and the sum of the background and reflection functions by the dashed histograms. The lower parts of the figures (with the indicated amplification factors) present the data and the results of the fit after subtracting the background and reflection contributions.

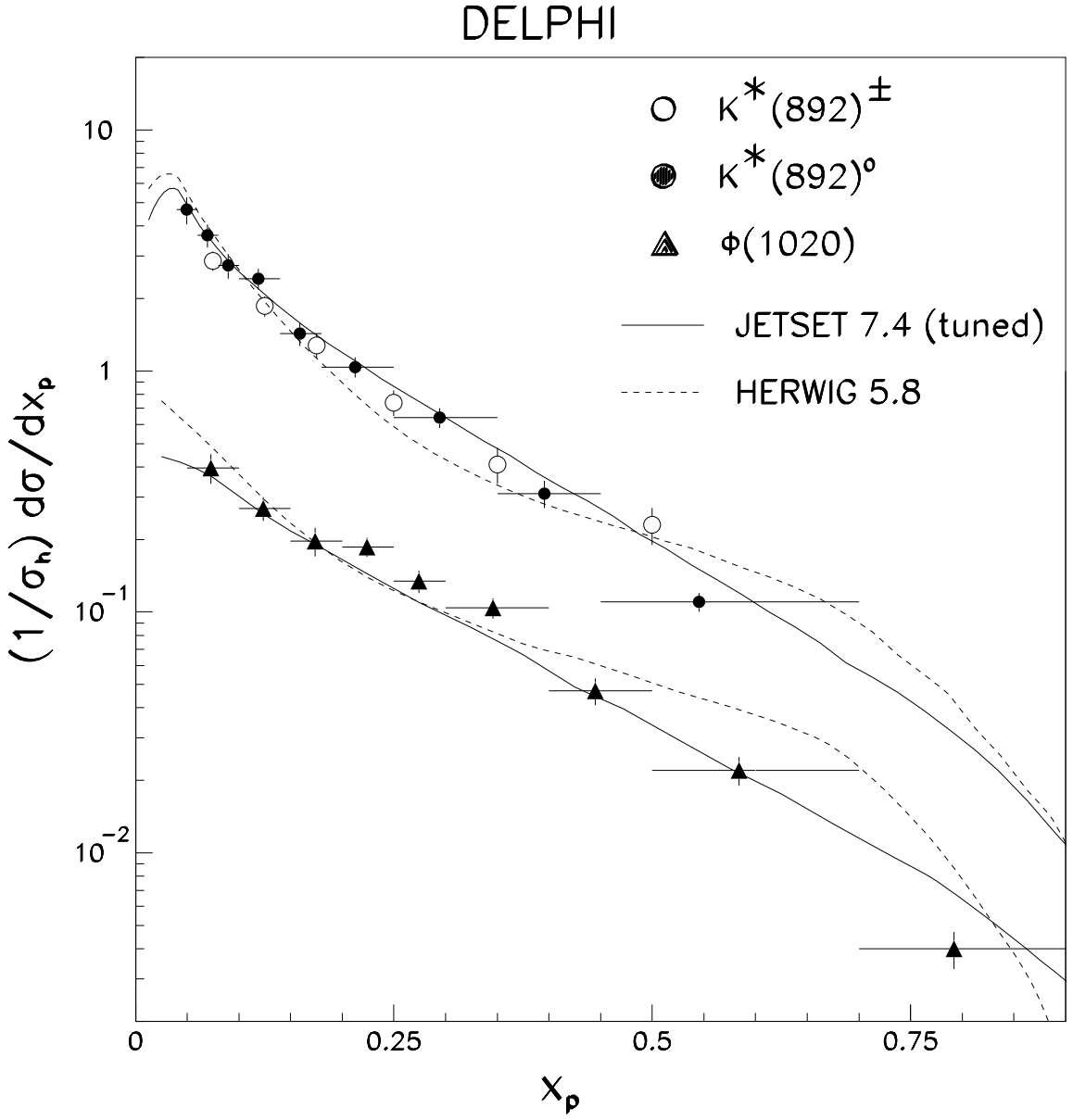

Figure 4: Differential cross sections $(1/\sigma_h)\cdot \mathrm{d}\sigma/\mathrm{d}x_p$ for inclusive $\mathrm{K}^{*0}(892)$, $\mathrm{K}^{*\pm}(892)$ and $\phi(1020)$ production measured by DELPHI. The statistical and systematic errors are combined quadratically. The points are plotted at the mean of the x_p values within the bin. The full and dashed curves respectively represent the expectations of the tuned JETSET 7.4 and HERWIG 5.8 for the $\mathrm{K}^*(892)$ and $\phi(1020)$.

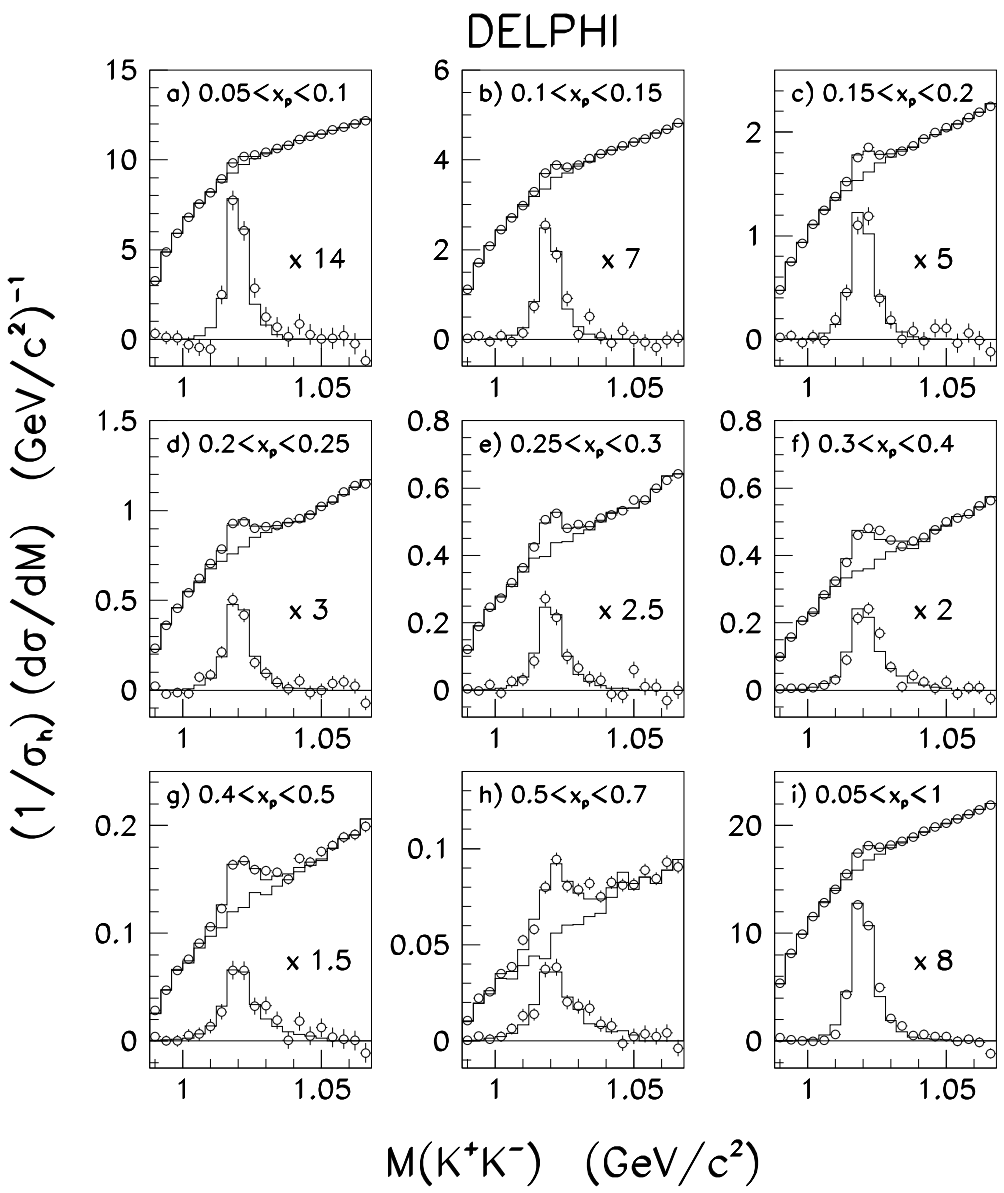

Figure 5: The K^+K^- invariant mass spectra for the indicated x_p-intervals for the uncorrected 1991-1994 data without particle identification (open points). The histograms are as in Fig. 3.

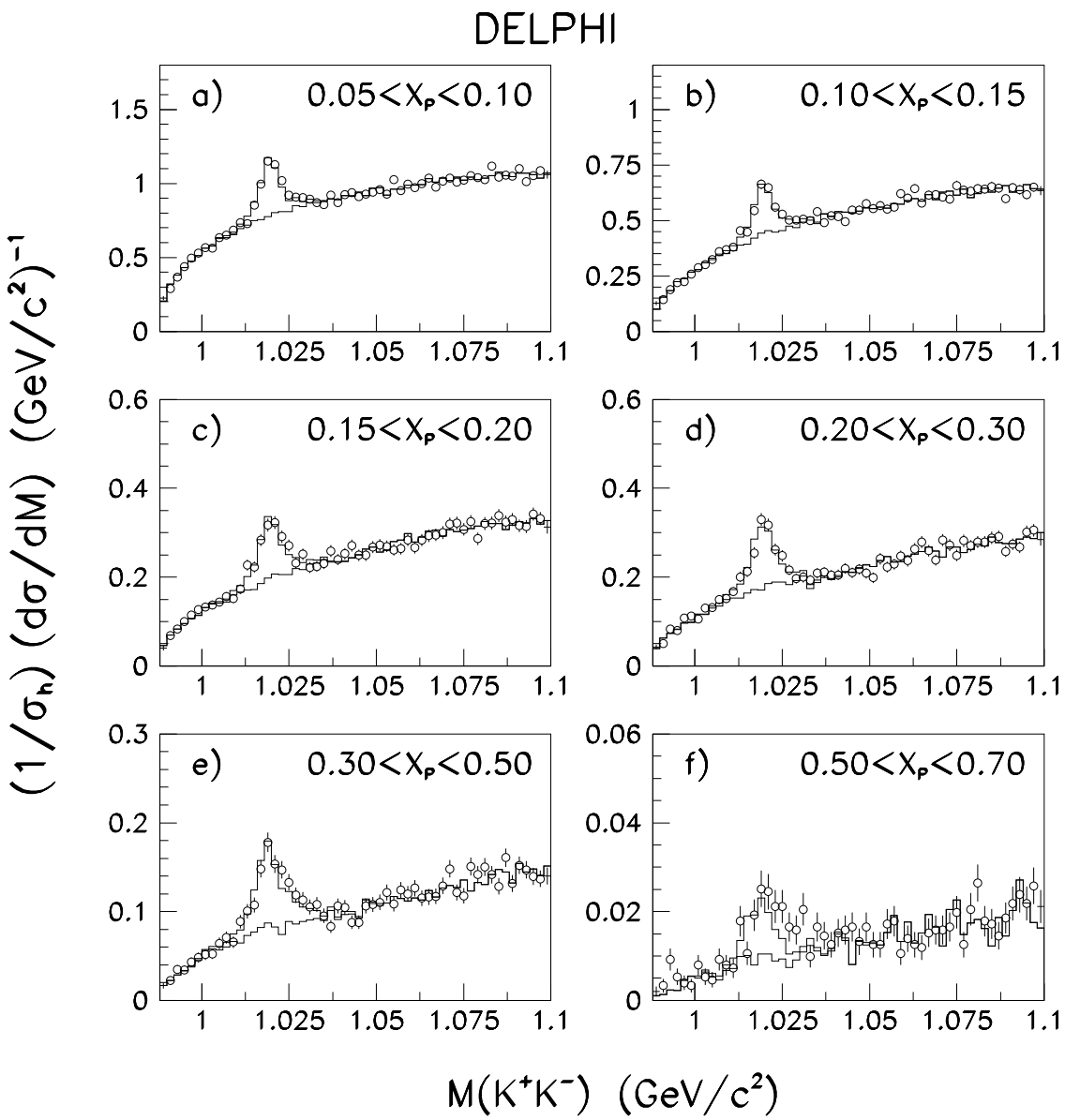

Figure 6: The K^+K^- invariant mass spectra for the indicated x_p-intervals for the uncorrected 1994 data with only one K in each K^+K^- pair required to be identified by the RICH detectors (open points). The upper histograms are the results of the fit. The background is shown by the lower histograms.

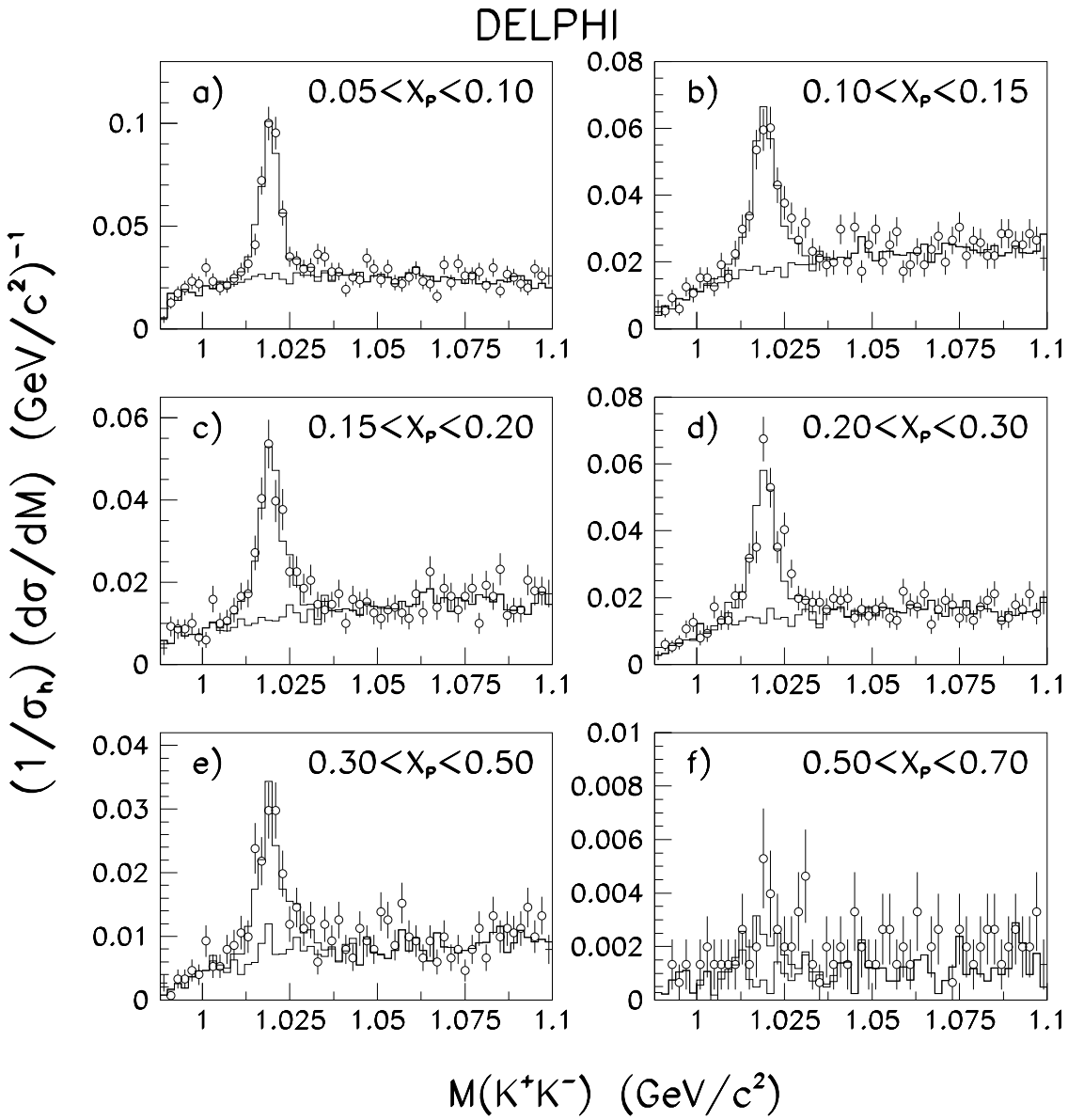

Figure 7: The K^+K^- invariant mass spectra for the indicated x_p-intervals for the uncorrected 1994 data with both kaons in each K^+K^--pair required to be identified by the RICH detectors (open points). The upper histograms are the results of the fit. The background is shown by the lower histograms.

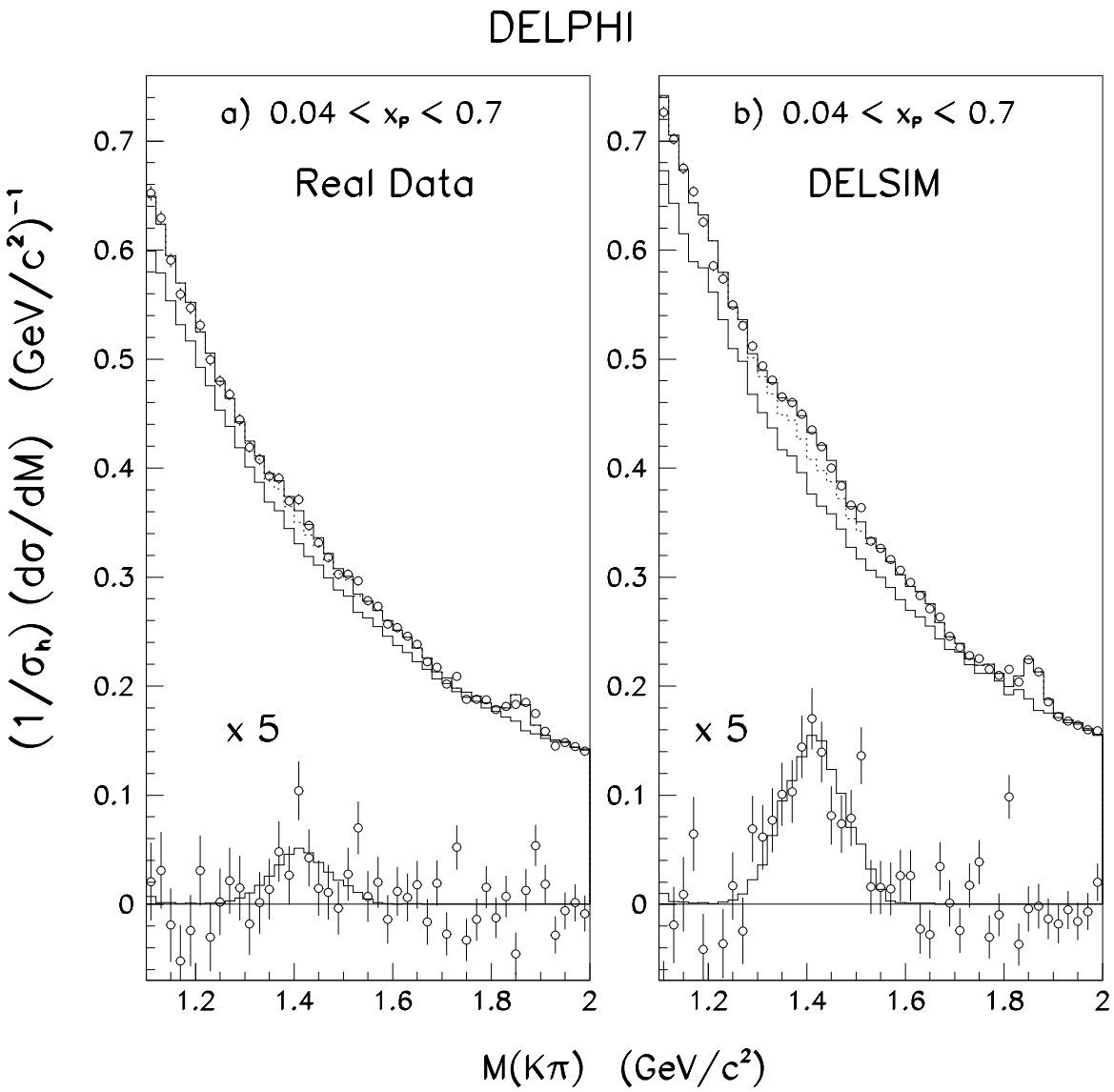

Figure 8: The $K^{\pm}\pi^{\mp}$ invariant mass spectra for the full measured $0.04 \leq x_p \leq 0.7$ range (open points) for the real (a) and simulated (b) data. The histograms are as in Fig. 3.